CHAPTER 6

Magnetic modulation in heteroallene and heterocumulene based *tert*-butyl nitroxide diradicals: spin delocalization and conformation play crucial roles

Abstract

We have theoretically investigated the magnetic property of heteroallene (>C=C=X−) and heterocumulene (>C=C=C=X−) based *tert*-butyl nitroxide diradicals (X is P/As). Calculation of magnetic exchange coupling constant (*J*) shows ferromagnetic interaction in heteroallene based diradicals. Whereas, in heterocumulene based diradicals, tuning of *J* value from antiferro- to ferro-magnetic state is observed from *Z*- to *E*- isomer. The essence of all findings is further explored by structural effects, spin density distribution and molecular orbital analysis. Delocalization of spin density from radical site to the coupler (in planar arrangement) is observed in spin distribution analysis. Moreover, the shapes of singly occupied molecular orbitals (SOMOs) advocate the delocalization of spin from radical center to the coupler. The typical feature of *tert*-butyl nitroxide radical creates spin delocalization along with spin polarization within the coupler. The *J* value of all diradicals strongly depends on the dihedral angle between radical center and coupler. The presence of heteroatom within the coupler produces major geometrical change that results magnetic crossover in heterocumulene based systems. Magneto-structural correlation shows that the change in dihedral angle tunes the magnetic property for both the *Z*- and *E*- isomers of heterocumulenes depending on the spin accumulation on two nearby magnetic centers. The energy gap between two consecutive SOMOs also supports this observation.

6.1 Introduction

Allene and cumulenes show interesting shapes and fascinating properties depending on the number of carbon atoms in the backbone chain[1,2] and have two types of π-bonds orthogonal to each other along their molecular axis. As allene and even cumulenes (containing even number of carbons) are structurally dissimilar, when the groups on end carbons are different, allene derivatives are chiral, whereas even cumulene derivatives show *Z*/*E* isomers.[3,4] Synthesis of long chain cumulenes and their characterization have been done by many researchers.[4-7]

There is a recent resurgence in studies relating to the switching of magnetic nature between ferromagnetic and antiferromagnetic states.[8-12] Normally the exchange interaction between two magnetic centers depends on the distance between radical centers as well as on the nature of the couplers.[13-15] However the interaction may follow different mechanisms[16] such as direct exchange, super exchange, ligand mediated exchange and so on. To search for excellent magnetic materials, the interaction between two magnetic centers connected through various couplers (such as conjugated chains and aromatic couplers) have been studied by different research groups.[13,17-22] In our previous works we have investigated the magnetic property of diradicals based on chiral allene as well as cumulene couplers and observed an anomalous magnetic behavior compared to the diradical based on conjugated systems.[23,24] Helical molecular orbitals of allene and cumulenes (with even number of double bonds) are investigated by notable researchers[25-27] and these systems can be tailored for use in enantioselective reactions.

Synthesis of heteroallenes,[28-31] in which one or more carbons are replaced by heavier elements of group 14 or 15, is a challenge in organometallic chemistry. Moreover heteroallene and heterocumulene (with 4 atoms in backbone chain) containing double bonded heavy elements, have attracted interest from a theoretical point of view because of their peculiar physicochemical properties.[29,32] Various types of phosphaallenes and phosphacumulenes −P=C=A (A=CR_2, PR, NR, C=PR, C=CR_2) have also been reported.[28,29] Märkl et al. in 1986 have synthesized phosphabutatriene −P=C=C=C< for the first time, a derivative with three cumulative double bonds.[33] On the other hand, though the stabilization of 1-arsabutatriene −As=C=C=C< is somewhat difficult due to the large size of arsenic, 1-Arsaallenes −As=C=C< have been first reported by Bouslikhane et al. which is stable towards air and moisture.[34] In the present study we have designed diradicals based on heteroallene (>C=C=X−) and heterocumulene (>C=C=C=X−) coupler where X is P/As.

The presence of heteroatom in the exchange pathway significantly influences magnetic exchange coupling.[35-37] Rancurel et al. have shown that the magnetic exchange between radical centers becomes more fragile when a heteroatom is introduced in the exchange pathway.[35] It is noted that when P atom bridges between

aminoxyl radical, exchange interaction depends on whether there is a participation of lone pair on P or not.[35] On the other hand, Polo et al. have opined that the introduction of heteroatom within the coupler may produce two or more inequivalent spin coupling pathways and the prediction of magnetic exchange interaction becomes more complicated.[36] Bhattacharya et al. investigated the spin leakage phenomenon of certain phosphoverdazyl systems and its effect on magnetic exchange coupling.[37] Herein, we are motivated to evaluate the potential effect of P/As atom substitution within the allene and cumulene couplers in mediating the exchange interaction between the two radical centers.

There are a number of stable organic radicals that are synthesized during last few decades.[38-43] Besides, lot of studies have been done predicting the magnetic property of molecules based on the *tert*-butyl nitroxide radical.[44-49] In the present investigation, we select the *tert*-butyl nitroxide as a spin source connected to heteroallene (>C=C=X−) and heterocumulene (>C=C=C=X−) coupler (X is P/As) and the systems studied are shown in Figure 6.1. The magnetic nature of these systems is quantified in DFT framework. The magnetic characteristics are rationalized through structural effects, spin density distributions, molecular orbital analysis and magneto-structural correlation.

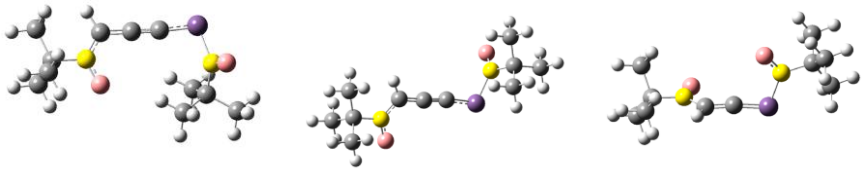

1(a) (Z-isomer) **1(b)** (E-isomer) **3**(Chiral)

P-substituted cumulene and allene based diradicals

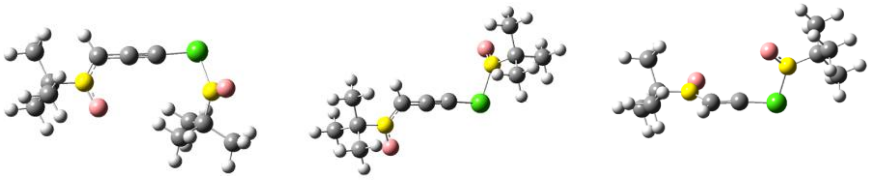

2(a) (Z-isomer) **2(b)** (E-isomer) **4**(Chiral)

As-substituted cumulene and allene based diradicals

Figure 6.1 Designed heteroallene and heterocumulene based diradicals where 1(a) and 1(b) represent *Z*- and *E*-isomer of P-substituted heterocumulene based diradicals, 2(a) and 2(b) represent *Z*- and *E*-isomer of As-substituted heterocumulene based diradicals, 3 and 4 represents the P- and As-substituted allene based diradicals. [Carbon, hydrogen, nitrogen, oxygen, phosphorus and arsenic atoms are depicted in grey, white, yellow, pink, purple, and green respectively].

6.2 Theoretical Background and Computational Strategy

For a system with two magnetic centers 1 and 2, the magnetic exchange interaction can be expressed by the phenomenological Heisenberg spin Hamiltonian $\hat{H} = -2J\hat{S}_1 \bullet \hat{S}_2$, where *J* is the effective exchange coupling constant between two magnetic centers of a diradical and $\hat{S}_1$ and $\hat{S}_2$ are the respective spin angular momentum operators. Positive sign of *J* indicates that the coupling is ferromagnetic and a negative value of *J* signifies the antiferromagnetic interaction in the diradical. For a diradical containing single unpaired electron on each magnetic site, *J* can be written as $E_{(S=1)} - E_{(S=0)} = -2J$.

Though the multiconfigurational approaches are suitable to describe pure spin states in an appropriate manner, these methods are not employed in this work as they are resource intensive. A more effective and useful alternative way with less computational effort is the Broken symmetry (BS) approach given by Noodleman et al.[50-53] in DFT framework. Many researchers have given different formulae for *J*.[54-56] However, the spin projected formula for the estimation of *J* has been given by Yamaguchi,[57-60] which is broadly applied and we also use this formula in this work $J = (E_{BS} - E_{HS}) \Big/ \left(\left\langle S^2 \right\rangle_{HS} - \left\langle S^2 \right\rangle_{BS} \right)$, where E_{HS}, E_{BS} and $\langle S^2 \rangle_{HS}$, $\langle S^2 \rangle_{BS}$, are the energy and average spin square values of corresponding high-spin and BS states.

Here, the molecular geometries of all the designed diradicals are fully optimized by hybrid exchange-correlation functional B3LYP, M06 and CAM-B3LYP (to include long range correction) using 6-311++G(d,p) basis set within unrestricted formalism. The open shell broken symmetry (BS) singlet solution has been obtained by using "guess=(read,mix)" keyword for mixing of HOMO and LUMO. Based on the energies of the triplet and the BS states at the same level of theory, *J* values of each molecule can be estimated using the spin projected formula given by Yamaguchi. Frequency calculation of all the diradicals gives positive values confirming that all the geometries are in local minima. Geometrical parameters of all the diradicals, the spin density distribution, and molecular orbital analysis are performed with the optimized geometry. All the calculations have been done by Gaussian 09 package.[61]

6.3 Result and Discussion

Magnetic exchange coupling constant

J values of all the designed diradicals are given in Table 6.1 Table 6.2 and Table 6.3 that are estimated using different exchange-correlation functionals (B3LYP, M06 and CAM-B3LYP) along with 6-311++G(d,p) basis set.

Table 6.1 The estimated energies (in a.u.) of triplet (T) state and broken symmetry (BS) state, corresponding $\langle S^2 \rangle$ values, and magnetic exchange coupling constant (*J*, in cm^{-1}) for all the diradicals (B3LYP/6-311++G(d,p)).

Diradicals	**$E_{(T)}$ ($\langle S^2 \rangle$)**	**$E_{(BS)}$ ($\langle S^2 \rangle$)**	***J* (cm^{-1})**
1(a) (*Z*–)	-1031.93594 (2.074)	-1031.93691 (1.011)	-200.27
2(a) (*Z*–)	-2926.44012 (2.065)	-2926.44051 (1.019)	-81.83
1(b) (*E*–)	-1031.93496 (2.074)	-1031.93427 (1.075)	151.59
2(b) (*E*–)	-2926.43915 (2.066)	-2926.43881 (1.059)	74.10
3	-993.83964 (2.054)	-993.83759(1.029)	440.0
4	-2888.33528 (2.067)	-2888.33305 (1.030)	471.97

Table 6.2 The estimated energies (in a.u.) of triplet (T) state and broken symmetry (BS) state, corresponding $\langle S^2 \rangle$ values, and magnetic exchange coupling constant (*J*, in cm^{-1}) for all the diradicals (M06 /6-311++G(d,p)).

Diradicals	**$E_{(T)}$ ($\langle S^2 \rangle$)**	**$E_{(BS)}$ ($\langle S^2 \rangle$)**	***J* (cm^{-1})**
1(a) (*Z*–)	-1031.41156 (2.068)	-1031.41288 (0.980)	-266.28
2(a) (*Z*–)	-2925.84247 (2.055)	-2925.84315(0.983)	-139.22
1(b) (*E*–)	-1031.40956 (2.071)	-1031.40907(1.054)	105.75
2(b) (*E*–)	-2925.83945(2.058)	-2925.83933(1.028)	24.54
3	-993.34352 (2.074)	-993.34048 (1.032)	640.65
4	-2887.76406(2.085)	-2887.76125(1.032)	585.68

Table 6.3 The estimated energies (in a.u.) of triplet (T) state and broken symmetry (BS) state, corresponding $\langle S^2 \rangle$ values, and magnetic exchange coupling constant (*J*, in cm^{-1}) for all the diradicals (CAM-B3LYP /6-311++G(d,p)).

Diradicals	**$E_{(T)}$ ($\langle S^2 \rangle$)**	**$E_{(BS)}$ ($\langle S^2 \rangle$)**	***J* (cm^{-1})**
1(a) (*Z*–)	-1031.56284 (2.156)	-1031.56360 (1.121)	-160.49
2(a) (*Z*–)	-2926.15818 (2.134)	-2926.15857 (1.107)	-83.34
1(b) (*E*–)	-1031.56149 (2.159)	-1031.56097 (1.156)	114.15
2(b) (*E*–)	-2926.15692 (2.139)	-2926.15654 (1.137)	83.23
3	-993.49053 (2.087)	-993.48833 (1.048)	464.72
4	-2888.07629 (2.115)	-2888.07376 (1.055)	523.84

There are certain issues associated with the calculated results that are discussed below.

(i) *J* values of heterocumulene based diradicals (isomers of 1 and 2) predict antiferromagnetic interaction in *Z*-isomers, while ferromagnetic interaction is observed in *E*-isomers. (ii) The magnitude of *J* value of heteroallene based diradicals (molecules 3 and 4) is higher than the heterocumulene based diradicals (isomers of 1 and 2 respectively), which is in contradiction to our previous study[24] where we have found that odd cumulene based diradicals have lesser magnitude of *J* value than that of the even cumulene based diradicals.

These observations demand a detailed investigation on the basis of the electronic structure analysis of the diradicals which are discussed in subsequent sections.

6.3.1 Structural characters and effects

Small changes in molecular structure can alter the *J* value significantly.[62] The strength of magnetic interaction depends on the distance between radical centers as well as the dihedral angle between radical center and coupler.[63-65] In this work, molecular structures of all the designed diradicals have been studied to understand their magnetic behavior.

6.3.1.1 Distance between radical centers

The extent of magnetic interaction is known to vary with the distance (*r)* between the magnetic centers as *exp*(-*r*).[66] For our designed systems (in Figure 6.1) the distance between radical centers are given in Table 6.4.

Table 6.4 Distance between radical centers *r* (in Å) for all the designed diradicals (using B3LYP/6-311++G(d,p)).

Systems	*r*	*J* (cm^{-1})	Systems	*r*	*J* (cm^{-1})
1(a) (*Z*-)	5.585	–200.27	2(a) (*Z*-)	5.622	-81.83
1(b) (*E*-)	6.858	151.59	2(b) (*E*-)	7.027	74.10
3	4.608	440.0	4	4.643	471.97

Table 6.4 shows that the distance between two radical centers increases from *Z*-isomer to *E*- isomer (in isomers of 1 and 2); consequently the magnitude of *J* value of *E*–isomers (1(b) and 2(b)) is lower than that of *Z*-isomers (1(a) and 2(a) respectively). The distance between radical centers of heteroallene based diradicals (3 and 4) are smaller compared to the respective heterocumulene based diradicals (isomers of 1 and 2 respectively) indicating the greater magnitude of *J* in heteroallene based diradical.

Photomagnetic crossover of several diradicals has already investigated where the trans-isomers are antiferromagnetic but cis-isomers are ferromagnetic (owing to the close proximity between radical centers that results direct exchange).[8] However for our designed *E*-isomer of heterocumulene based diradicals, the distance between two radical centers is sufficiently large (i.e., 6.858 Å for 1(b) and 7.027 Å for 2(b)), so a significant through-space direct exchange interaction between them is unlikely. Therefore the change in the sign of *J* value from *Z*- to *E*-isomer needs to be ascertained from some other criterion.

6.3.1.2 Dihedral angle

Several studies show that the magnitude of *J* strongly depends on the planarity of the molecular structure.[64,65] In one of our previous studies, we have shown that the coupling constant values of even cumulene based diradicals are higher than odd cumulene based diradicals; as for the later systems two radical centers are in perpendicular plane, while in former cases the radical centers are in the same plane.[24] In this work, the dihedral angle ϕ (q-r-r′-q′) between two radical centers R_1 and R_2 (considering only the connecting nitrogen atoms of two radical centers R_1 and R_2) shows that in heterocumulene based diradicals, the two N atoms of two radical centers are almost in same plane and in heteroallene based diradicals, the two N atoms of two radical centers are in perpendicular plane (given in Table 6.5). However the magnitude of *J* in heteroallene based diradicals is higher compared to heterocumulene based diradicals. To understand the fact we analyze the dihedral angle φ_1 (between R_1

and coupler) and φ_2 (between R_2 and coupler) in heterocumulene and heteroallene systems (in Figure 6.2) as given in Table 6.5.

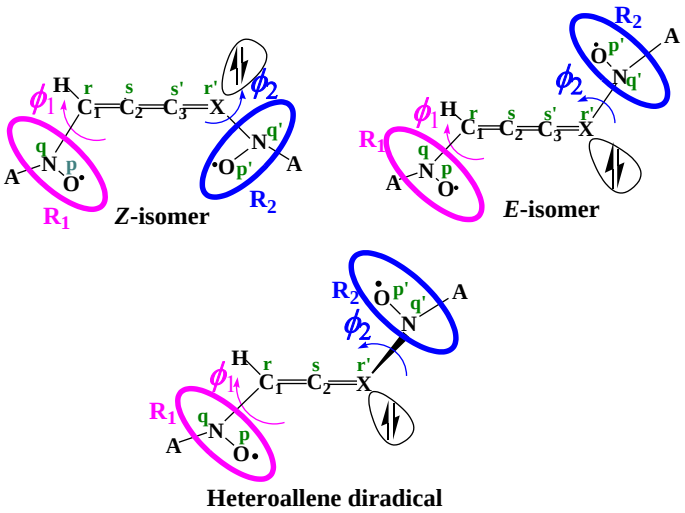

Figure 6.2 $\varphi_1$and φ_2 denote the dihedral angle between the plane of coupler and that of the nitroxide radicals (R_1 and R_2 respectively) and X denotes P/As, A stands for $-C(CH_3)_3$. R_1 and R_2 represents same radical center (–NO) but linked with different atoms (i.e., R_1 is connected to C_1 and R_2 is connected to X of the coupler).

Table 6.5 Dihedral angles from optimized geometry of heterocumulene and heteroallene based diradicals (using B3LYP/6-311++G(d,p)).

System	(Dihedral angle)°			J (cm^{-1})
	ϕ_1 (p-q-r-s)	ϕ_2 (p′-q′-r′-s′)	ϕ (q-r-r′-q′)	
1(a) (*Z*-)	–0.61	–104.11	–7.53	–200.27
1(b) (*E*-)	0.63	–93.97	176.43	151.59
2(a) (*Z*-)	–0.63	–101.93	–11.57	-81.83
2(b) (*E*-)	0.48	–98.41	174.96	74.10
System	ϕ_1 (p-q-r-s)	ϕ_2 (p′-q′-r′-s)	ϕ (q-r-r′-q′)	J (cm^{-1})
3	2.41	3.63	94.52	440.0
4	2.70	3.80	94.65	471.97

Table 6.5 shows that in heterocumulene based diradicals, R_1 and coupler are in same plane (dihedral angle $\phi_1 \approx 0^o$). However the dihedral angle ϕ_2 could not afford the planarity between R_2 and coupler due to the presence of lone pair of electrons on heteroatom (P/As). So a reduced delocalization of electrons occurs between the coupler and radical center (R_2). The extent of non planarity increases from *Z*- to *E*-isomer (ϕ_2), resulting smaller magnitude of *J* for *E*-isomers than the *Z*-isomer. On the other hand though heteroallene coupler has two types of perpendicular π-planes, dihedral angle φ_1 and φ_2 show that the radical centers are almost in same plane with the coupler (given in Table 6.5). Consequently a better interaction between radical

center and the coupler occurs that results higher magnitude of *J* value in heteroallene based diradicals (3 and 4) compared to heterocumulene based diradicals (1 and 2).

6.3.2 Spin density distribution

Spin density distribution is an important factor that tunes the interaction between different magnetic sites and has an effect on the sign of *J* values.[13,14] Distribution of spin density on each atom of the coupler and on the radical centers of all the diradicals (in their optimized structure) are given in Table 6.6 and Table 6.7. The concerns associated with these results are discussed in the following.

Table 6.6 Spin density distribution on each atom of the coupler of *Z*- and *E*-isomers of heterocumulene based diradicals in their BS state and triplet state respectively (B3LYP/6-311++G(d,p)).

Systems	R_1	C_1	C_2	C_3	X (P/As)	R_2
1(a) (*Z*-)	0.4761	–0.1943	0.2985	–0.2079	0.5798	–0.9619
2(a) (*Z*-)	–0.3950	0.1880	–0.2807	0.2477	–0.7333	0.9780
1(b) (*E*-)	0.4868	–0.1949	0.2892	–0.2386	0.6611	0.9544
2(b) (*E*-)	0.4109	–0.1874	0.2704	–0.2245	0.7224	0.9788

(i) Spin density distribution (given in Table 6.6) on *Z*-isomers (1(a) and 2(a)) follow the spin alternation rule.[67] However an unexpected outcome is obtained in the spin distribution i.e., although the spin density on R_2 (−NO) is almost unity, spin density on R_1 (−NO) is far less than unity and a large accumulation of spin density is observed on the heteroatom (P/As).

(ii) For *E*-isomers (1(b) and 2(b)), spin density (given in Table 6.6) on R_1 (−NO) is also far below from unity and heteroatom (X) have a large accumulation of spin density. Furthermore, a regular alternation of the spin density occurs within the R_1 and the coupler but the alternation breaks between X (P/As) and R_2 (−NO).

(iii) In heteroallene based diradicals (3 and 4), spin density distribution (given in Table 6.7) follow spin alternation between radical centers and the coupler. Unlike a large accumulation of spin density on heteroatom (P/As) as observed in heterocumulene based diradicals (isomers of 1 and 2), large amount of spin density is observed on C_2 of heteroallene coupler (in Table 6.7) and the spin density on R_1 (−NO) and R_2 (−NO) decreases to some extent from unity.

Table 6.7 Spin density distribution on each atom of the coupler of heteroallene based diradicals in their triplet state (B3LYP/6-311++G(d,p)).

Systems	R_1	C_1	C_2	X (P/As)	R_2
3	0.7886	–0.2205	0.6783	–0.1539	0.8889
4	0.7845	–0.2513	0.7367	–0.2285	0.9352

Such distribution of spin density on all the diradicals is quite astonishing. To understand the unusual type of spin density distribution on the magnetic center and coupler, we have studied a set of P-substituted allene and cumulene based diradicals by changing the radical center, i.e., instead of *tert*-butyl nitroxide radical, nitronyl nitroxide radical is considered as spin center and the designed systems are given in Figure 6.3. The magnetic exchange coupling constant values for those nitronyl nitroxide diradicals are given in Table 6.8. The spin density distribution (given in Table 6.9 and Table 6.10) for all the nitronyl nitroxide diradicals show that the spin density on the radical sites is almost unity and the coupler has very small spin density compared to the radical units. Thus, the spin density distribution on our designed *tert*-butyl nitroxide diradicals (Figure 6.1) reveals striking differences from that of the nitronyl nitroxide based diradicals. From this observation we can conclude that the radical unit (*tert*-butyl nitroxide radical) has a major role in such unusual type spin density distribution.

P substituted cumulene and allene based nitronyl nitroxide diradicals

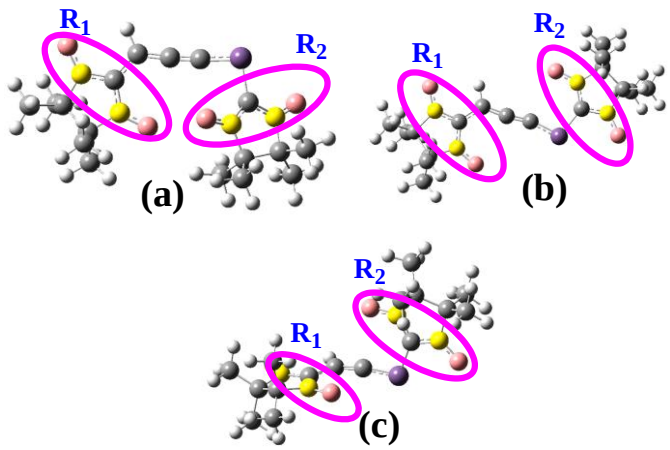

Figure 6.3 Designed nitronyl nitroxide diradicals based on heteroallene and heterocumulene couplers (with P-substitution). (a) and (b) represents *Z*- and *E*- isomer of heterocumulene based diradicals respectively, (c) represents the heteroallene based diradicals. [Carbon, hydrogen, nitrogen, oxygen, phosphorus atoms are depicted in grey, white, yellow, pink and purple respectively]. Here R_1 and R_2 (−NO−C−NO− group) are shown by magenta circle.

Table 6.8 The energy (a.u.),$\langle S^2 \rangle$ and magnetic exchange coupling constant (J in cm^{-1}) of all the nitronyl nitroxide diradicals (B3LYP/6-311++G(d,p)).

Diradicals	$E_{(T)}$ ($\langle S^2 \rangle$)	$E_{(BS)}$ ($\langle S^2 \rangle$)	J (cm^{-1})
S1(a) Z-	-1524.15524 (2.185)	-1524.15736 (1.309)	-529.76
S1(b) *E*-	-1524.15697 (2.144)	-1524.16057 (1.352)	-997.38
S1(c)	-1486.06429(2.149)	-1486.06405 (1.133)	52.62

From Table 6.8 it is observed that for heterocumulene based nitronyl nitroxide diradicals, both *Z*- and *E*- isomers show antiferromagnetic coupling and heteroallene based nitronyl nitroxide diradical shows ferromagnetic coupling as expected from spin density alternation rule.

Table 6.9 Spin density distribution on each atom of the coupler of *Z*- and *E*- isomers of P- substituted even cumulene based nitronyl nitroxide diradical in their BS state (B3LYP/6-311++G(d,p)).

Systems	**R_1 (−NO−C−NO−)**	**C_1**	**C_2**	**C_3**	**X**	**R_2 (−NO−C−NO−)**
S1(a) Z-	-1.1585	-0.2259	0.2055	-0.2234	0.3108	1.0489
S1(b) *E*-	-1.1820	-0.2486	0.1984	-0.2288	0.3030	1.1304

Table 6.10 Spin density distribution on each atom of the coupler of P- substituted allene based nitronyl nitroxide diradical in their high spin state (B3LYP/6-311++G(d,p)).

System	**R_1 (−NO−C−NO−)**	**C_1**	**C_2**	**X**	**R_2 (−NO−C−NO−)**
S1 (c)	1.0667	0.1173	-0.2831	0.0780	1.0548

Schatzschneider et al. have investigated that in *tert*-butyl phenyl nitroxides, a direct delocalization of unpaired electron occurs through the phenyl ring at the coplanar geometry and the delocalization decreases with increasing dihedral angle between radical group and phenyl ring.[68] The spin density distribution of *tert*-butyl nitroxide based diradicals (in Table 6.6 and Table 6.7) and of nitronyl nitroxide based diradicals (in Table 6.9 and Table 6.10) point out that in both the cases spin density spreads out onto the coupler. In nitronyl nitroxide diradicals, as the spin density on radical sites is almost unity (in Table 6.9 and Table 6.10), the delocalization of unpaired electrons of radical centers within the coupler is constrained. So, one can surmise that the spin density on the coupler arises from spin polarization within the coupler in nitronyl nitroxide diradicals.

For the heterocumulene based *tert*-butyl nitroxide diradicals (both *Z*- and *E*-isomers), dihedral angle (ϕ_1 in Table 6.5) suggest that R_1 (−NO) and the coupler are almost in same plane. Consequently along with the spin polarization, the additional contribution of spin density on the coupler and low contribution of spin density on R_1 is due to the spin delocalization (that occurs from the delocalization of unpaired electron between R_1 and the coupler as given in Table 6.6). However the dihedral angle (ϕ_2 in Table 6.5) between R_2 and coupler predict nonplanarity between them. The extent of delocalization of unpaired electron from R_2 to the coupler is negligible and the spin density on R_2 is almost one as seen in Table 6.6.

A plausible mechanistic pathway of the delocalization of unpaired electron from R_1 to the coupler is given in Figure 6.4. Here R_1 and the coupler together form one delocalized radical unit as shown by blue dotted line. The net magnetic coupling is due to the interaction between blue dotted radical unit and R_2. Similar delocalization of electron also observed in *E*-isomers. Table 6.6 shows that, at a certain dihedral angle (ϕ_2) in *E*-isomer, similar spin accumulates on two nearby magnetic centers that results ferromagnetic coupling. However in Z-isomer, antiferromagnetic coupling is observed owing to the opposite spin accumulation on two nearby magnetic centers (spin density plot is given in Figure 6.5 and Figure 6.6).

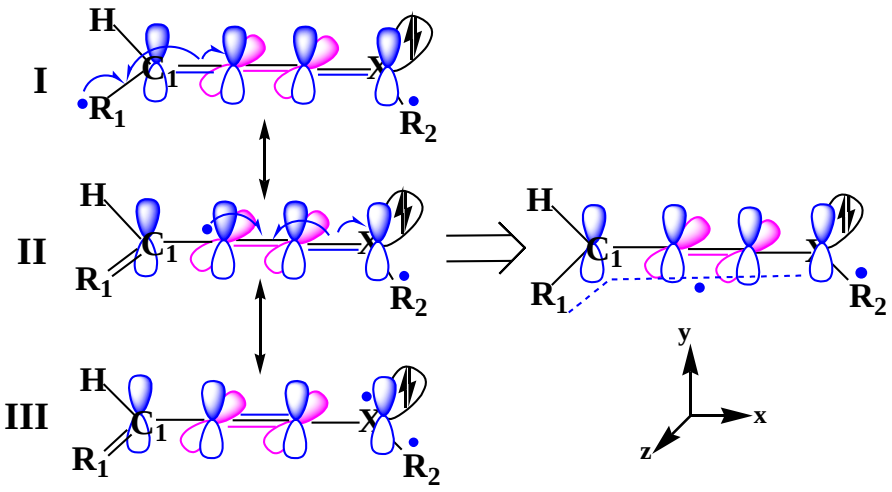

Figure 6.4 Delocalization of unpaired electron within the radical center (R_1) and the coupler in *Z*-isomer of heterocumulene based diradical. The magenta and blue lobes are two perpendicular *p* orbitals that form orthogonal π bonds in heteroatom substituted cumulene chain. Blue and magenta bonds are two perpendicular π bonds and blue arrows represents the electron delocalization pathways.

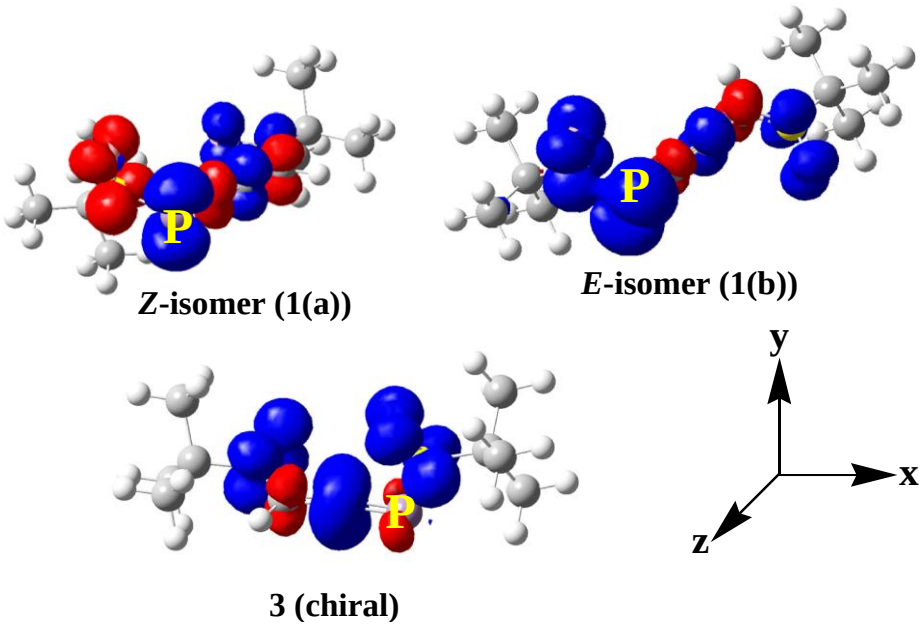

Figure 6.5 Spin density plot for the *Z*–isomer of P-substituted cumulene based *tert*-butyl nitroxide diradicals (BS states) and *E*– isomer of P-substituted cumulene based *tert*-butyl nitroxide diradical (high spin states) and P-substituted allene based *tert*-butyl nitroxide diradical (high spin states) using (B3LYP/6-311++G(d,p)), (iso value 0.004), red and blue colors represent the α and β spins respectively.

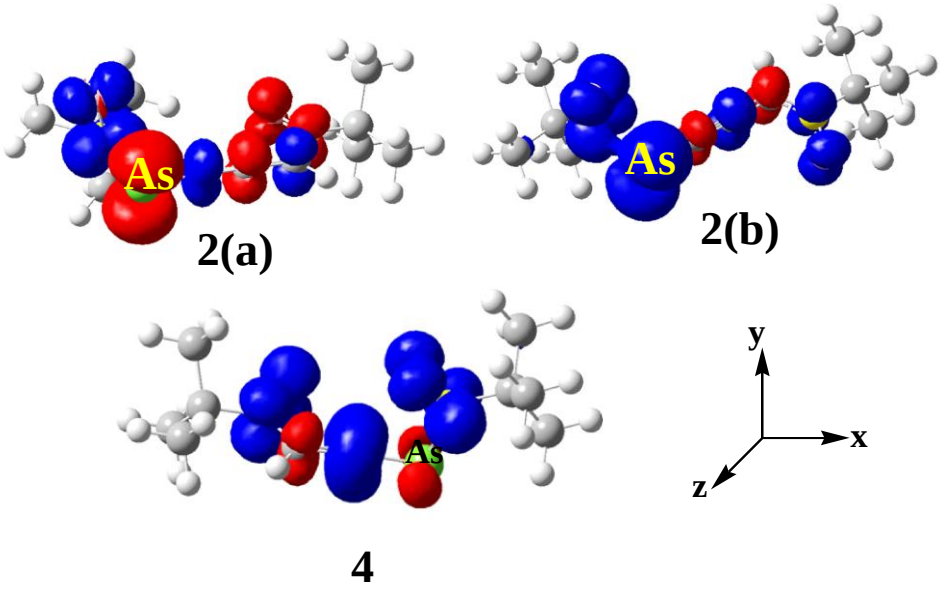

Figure 6.6 Spin density plot for the *Z*-isomer of As-substituted cumulene based *tert*-butyl nitroxide diradical (BS states) and *E*- isomer of As-substituted cumulene based *tert*-butyl nitroxide diradical (high spin states) and As-substituted allene based *tert*-butyl nitroxide diradical (high spin states) using (B3LYP/6-311++G(d,p)), (iso value 0.004), red and blue colors represent the α and β spins respectively.

For the heteroallene based diradicals, R_1 and the coupler are in same plane as observed from dihedral angle (ϕ_1 in Table 6.5). The delocalization of unpaired electron from R_1 to the coupler occurs smoothly which is shown in Scheme 1 of Figure 6.7. But the delocalization does not proceed beyond C_2, due to the presence of perpendicular π bonding orbital. Similarly, dihedral angle (ϕ_2 in Table 6.5) between coupler and radical center (R_2) shows that they are in almost same plane. The delocalization of unpaired electron occurs from R_2 to C_2 as shown in Scheme 2 of Figure 6.7. These two pathways collectively increase the spin density on C_2. Now the magnetic coupling is the result of the interaction between R_2 and blue dotted radical unit via the heteroatom.

The blue and magenta lobes are two orthogonal *p* orbitals in heteroallene chain and the blue and magenta dotted lines are two different electron delocalization pathways that are shown in Figure 6.7.

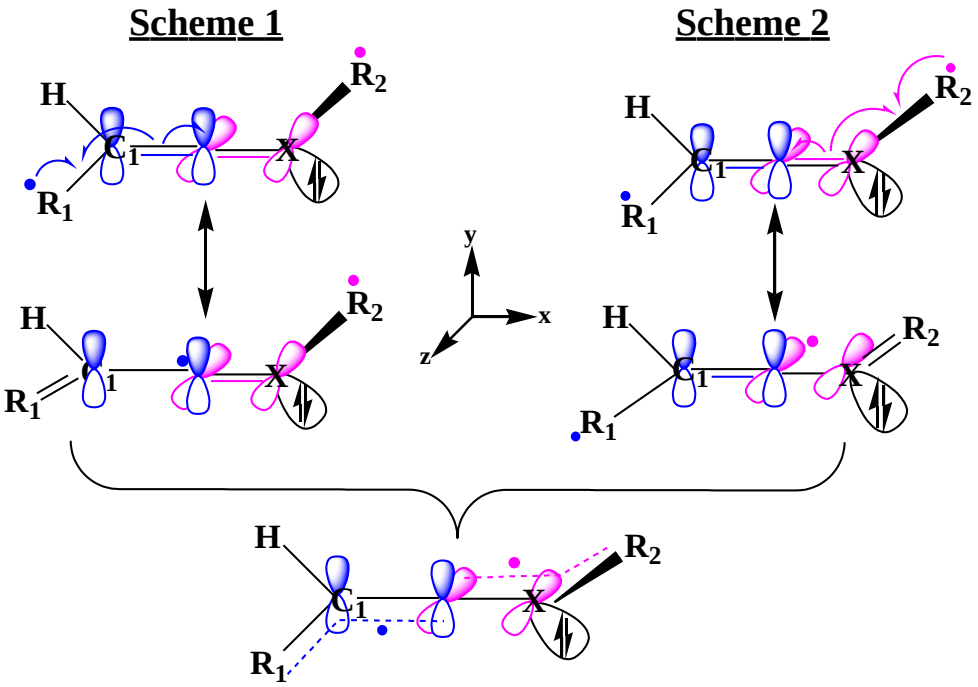

Figure 6.7 Delocalization of unpaired electron within the radical centers and coupler in heteroallene based diradicals.

6.3.3 Magneto-structural correlation

Though the *Z*- and *E*-forms are geometrical isomers that differ primarily by dihedral angle, the crossover of *J* values in heterocumulene based diradicals is quite interesting. Fang et al. have investigated that, if *tert*-butyl nitroxide radicals are twisted out of conjugation with the m-phenylene linker, the ability of ferromagnetic coupling reduces and antiferromagnetism arises depending on the dihedral angle between m-phenylene and the nitroxyl group.[46] Here we want to clarify how the dihedral angle ϕ_2 (Figure 6.2) affect the spin coupling between radical centers for both the P-substituted isomers of heterocumulene based diradicals. On the optimized geometry of 1(a) and 1(b) (using B3LYP/6-311++G(d,p)), single point calculation is done by changing the dihedral angle(ϕ_2) between –60º to –110º (at the same level of theory) with 10º interval. The change in magnetic exchange coupling constant value (*J*) with respect to the dihedral angle (φ_2) for both the isomers is given in Figure 6.8.

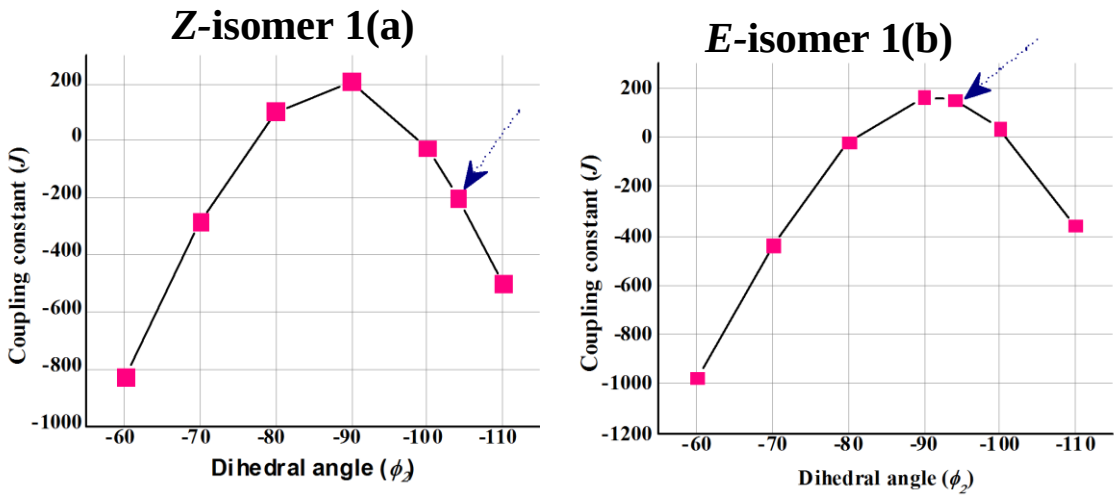

Figure 6.8 Coupling constant values (*J*, in cm^{-1}) of *Z*-isomer and *E*-isomer of P-substituted cumulene based diradicals by varying dihedral angle (φ_2, in degree) between the radical (R_2) and the coupler (B3LYP/6-311++G(d,p)).

Figure 6.8 clearly shows that for both the *E*- and *Z*-isomers (1(a) and 1(b)), a decreasing trend of antiferromagnetic *J* value is observed when twisting the dihedral angle φ_2 from –60º. A magnetic crossover between antiferro- and ferro-magnetic states occurs (for both the isomers) in the way of twisting the dihedral angle (ϕ_2) ≈ –80º and –100º. Hence we notice that ϕ_2 values are instrumental in tuning the *J* values. However the optimized geometry of *Z*-isomer has the ϕ_2 value –104.11º (in Table 6.5) which results antiferromagnetic coupling (shown in Figure 6.8 by a blue dotted arrow). Whereas, the optimized geometry of *E*-isomer shows that the ϕ_2 value is –93.97º (in Table 6.5) and a ferromagnetic coupling results (shown by a blue dotted

arrow in Figure 6.8). Thus from this section it is clear that a small change in dihedral angle in *Z*- and *E*-isomer is the major reason for the tuning of *J* values.

6.3.4 Molecular orbital analysis

In Section 6.3.2 we have interpreted that R_1 and coupler together form a delocalized radical unit which exhibits magnetic coupling with the other radical unit R_2 in heterocumulene based diradicals. To further justify this analysis, we scrutinize the molecular orbitals of all the P-substituted cumulene based diradicals (1(a) and 1(b)) that are sketched in Figure 6.9.

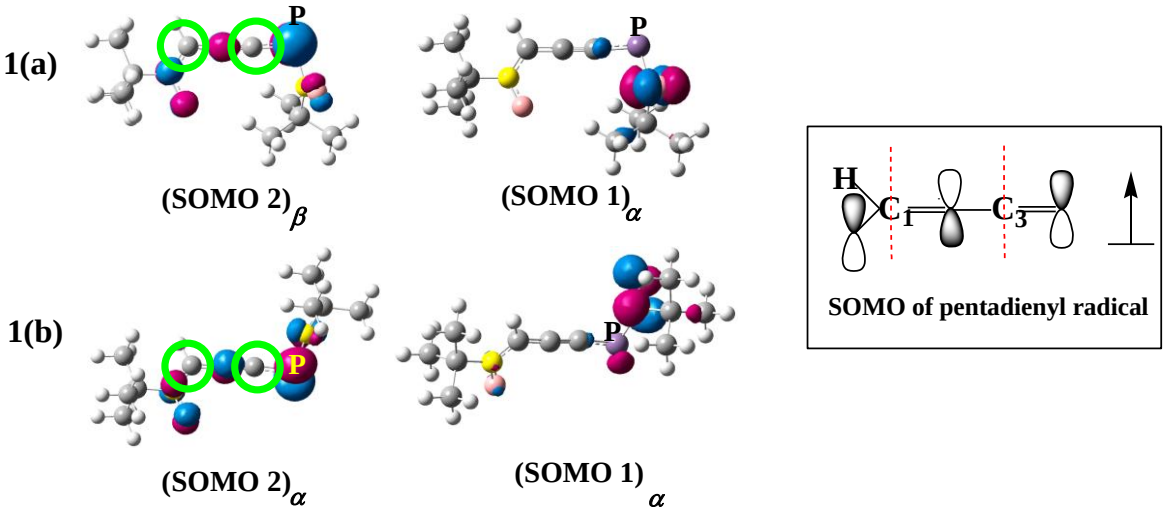

Figure 6.9 Spatial distribution of SOMOs of all the P-substituted cumulene based diradicals (1(a) and 1(b)) (B3LYP/6-311++G(d,p)) (iso value 0.06), blue and dark pink colors represent the different phase of the orbital coefficients. Within the inset, the SOMO of pentadienyl radical are shown. The red dotted lines represent nodal planes on C_1 and C_3.

It is clear from Figure 6.9 that, for both the *Z*- and *E*- isomers of P-substituted even cumulene based diradicals, SOMO1 is mostly located on the radical center R_2 and SOMO2 is mostly on the radical center R_1 as well as on the coupler. On the other hand, the molecular orbital analysis of nitronyl nitroxide based diradicals (specifically designed for comparison purpose as mentioned earlier and results are given in Figure 6.10) shows that the two SOMOs are centered exclusively on the radical centers. So the delocalization of unpaired electron is again confirmed from the MO analysis in *E*- and *Z*- isomers of P-substituted cumulene based *tert*-butyl nitroxide diradicals (1(a) and 1(b)).

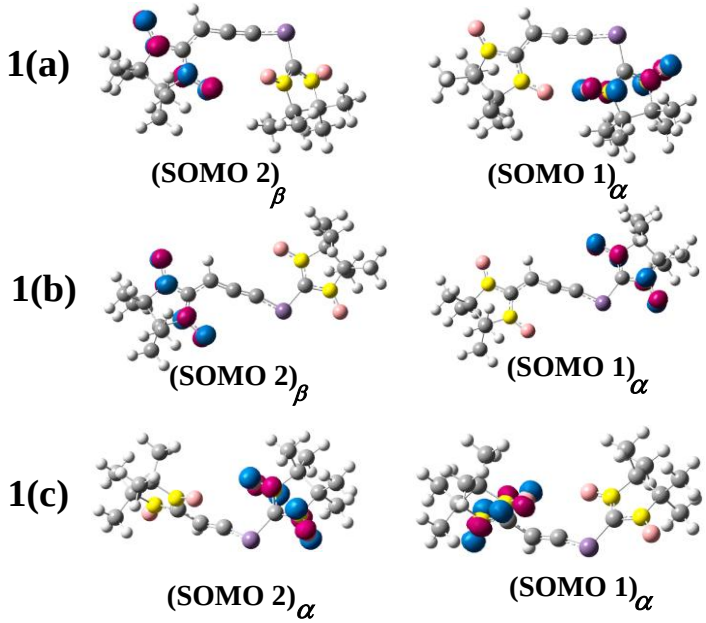

Figure 6.10 Spatial distribution of molecular orbitals of the P-substituted allene and cumulene based nitronyl nitroxide diradicals (B3LYP/6-311++G(d,p)) (iso value 0.06), blue and dark pink colors represent the different phase of the orbital coefficients.

Another notable point is that, SOMO2 of both 1(a) and 1(b) has two nodal points on C_1 and C_3 (green circle in Figure 6.9). If we consider the delocalization of unpaired electron from radical center R_1 to coupler (in Figure 6.4), it has the similar structure as that of SOMO of pentadienyl radical (inset in Figure 6.9). This observation confirms the mechanism of electron delocalization in our designed cumulene based systems. Similar analogy can also be put forward in case of As-substituted diradicals (2(a) and 2(b)) given in Figure 6.11.

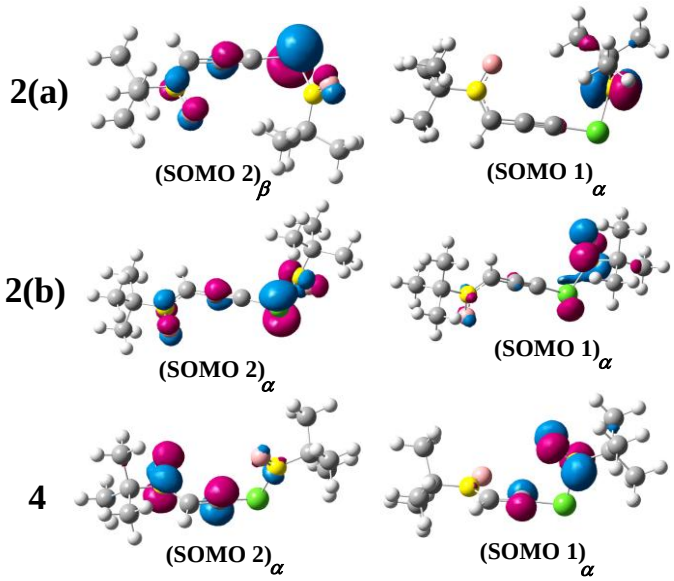

Figure 6.11 Spatial distribution of molecular orbitals of all the As-substituted cumulene and allene based *tert*-butyl nitroxide diradicals (B3LYP/6-311++G(d,p)) (iso value 0.06), blue and dark pink colors represent the different phase of the orbital coefficients.

For P-substituted allene based diradical (molecule 3 in Figure 6.1), SOMO2 has large coefficients on the radical center R_1 as well as on the coupler (on C_2) shown in Figure 6.12. Similarly SOMO1 has large coefficients on the R_2 as well as on the coupler (on C_2). The molecular orbital analysis again confirms the delocalization of radical unit as both the SOMOs spread over the radical center as well as the coupler. Moreover SOMO2 and SOMO1 have nodal points on C_1 and C_3 respectively (green circle in Figure 6.12). If we consider the SOMO of allyl radical, it has the well-known form shown in the inset of Figure 6.12 which has also one nodal point. This observation confirms the mechanism of electron delocalization between radical center and coupler (in two different planes) similar to that of the allyl radical. The molecular orbital of As-substituted allene based diradical is given in Figure 6.11.

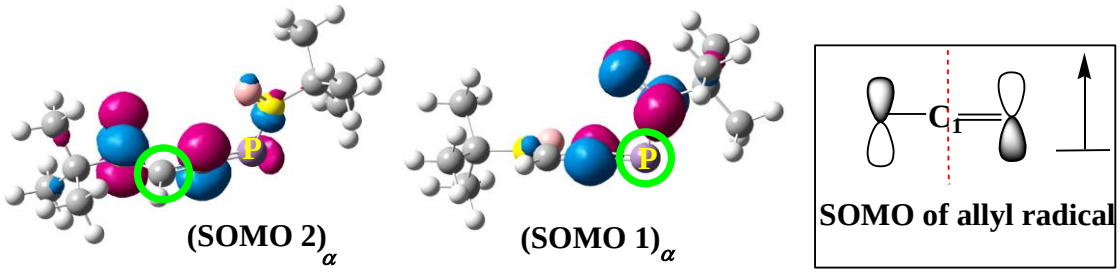

(SOMO 2)$_\alpha$ (SOMO 1)$_\alpha$

Molecule (3)

Figure 6.12 Spatial distribution of SOMOs of the allene based diradicals with P-substitution (B3LYP/6-311++G(d,p)) (iso value 0.05), blue and dark pink colors represent the different phase of the orbital coefficients. Within the inset, the SOMO of allyl radical are shown. The red dotted line represents nodal plane on C_1.

To understand the crossover of *J* value with change in dihedral angle (ϕ_2), we analyze the energy difference between two consecutive SOMOs of 1(a) and 1(b) at different dihedral angles given in Table 6.11. Frontier molecular orbital (FMO) energies of 1(a) and 1(b) are given in Table 6.12 and Table 6.13. According to Hoffmann[69] if the energy difference between two consecutive SOMOs is less than 1.5 eV, electrostatic repulsion between two degenerate orbitals increases and a spin-parallel orientation occurs with a triplet ground state. The critical value of ΔE_{SS} can be different for different systems.[70] From Table 6.11 it is clear that for both the 1(a) and 1(b), the ΔE_{SS} value decreases with change in φ_2 value from –60º to –90º and after that the ΔE_{SS} value increases with the change in φ_2 value. For *Z*-isomer, ΔE_{SS} value reaches to a minimum value at ϕ_2 value –80º and –90º, resulting a ferromagnetic coupling. But our optimized geometry have the φ_2 value –104.11º, so the antiferromagnetic coupling for *Z*-isomer results that are shown in Table 6.11. On the other hand, in *E*-isomer of even cumulene based diradical, ΔE_{SS} value reaches to a minimum value at ϕ_2 value –90º and –100º and our optimized geometry shows the φ_2 value is –93.97º. As a result ferromagnetic coupling is observed in *E*-isomer (shown in Table 6.11).

Table 6.11 Dihedral angle (φ_2, in degree), Energy difference (SOMO1 (HOMO)$_\alpha$)–(SOMO2 (HOMO-1)$_\alpha$)(ΔE_{SS}) and magnetic exchange coupling constant (J) in their triplet state (B3LYP/6-311++G(d,p)). The results for optimized geometries are given in bold face.

***Z*-isomer (1(a))**			***E*-isomer (1(b))**		
(φ_2)	**ΔE_{SS} (eV)**	**J(cm^{-1})**	**(φ_2)**	**ΔE_{SS} (eV)**	**J(cm^{-1})**
–60	0.718	–828.34	–60	0.790	–974.91
–70	0.470	–284.91	–70	0.555	–440.32
–80	0.209	102.60	–80	0.307	–21.57
–90	0.074	205.70	–90	0.072	164.19
–100	0.335	–26.44	**–93.97**	**0.0832**	**151.59**
–104.11	**0.442**	**–200.27**	–100	0.224	36.782
–110	0.594	–500.99	–110	0.474	–358.32

Table 6.12 Energy (in a.u.) of (SOMO 2)$_\alpha$, (SOMO 1)$_\alpha$ and (LUMO)$_\alpha$ for *Z*-isomer of P-substituted cumulene based *tert*-butyl nitroxide diradicals (B3LYP/6-311++G(d,p)).

Dihedral angle (*Z*-isomer)	**(SOMO 2)$_\alpha$ (a.u.)**	**(SOMO 1)$_\alpha$ (a.u.)**	**(LUMO)$_\alpha$ (a.u.)**
-60º	-0.21833	-0.19195	-0.06811
-70º	-0.21444	-0.19718	-0.06902
-80º	-0.21021	-0.20253	-0.06986
-90º	-0.2082	-0.20549	-0.07067
-100º	-0.21341	-0.20112	-0.07147
-104.11º	-0.21556	-0.1993	-0.0718
-110º	-0.21855	-0.19674	-0.07222

Table 6.13 Energy (in a.u.) of (SOMO 2)$_\alpha$, (SOMO 1)$_\alpha$ and (LUMO)$_\alpha$ for *E*-isomer of P-substituted cumulene based *tert*-butyl nitroxide diradicals (B3LYP/6-311++G(d,p)).

Dihedral angle (*E*-isomer)	**(SOMO 2)$_\alpha$ (a.u.)**	**(SOMO 1)$_\alpha$ (a.u.)**	**(LUMO)$_\alpha$ (a.u.)**
-60º	-0.22067	-0.19164	-0.06798
-70º	-0.21672	-0.19631	-0.06873
-80º	-0.2125	-0.2012	-0.06941
-90º	-0.2085	-0.20585	-0.07009
-93.97º	-0.20883	-0.20577	-0.07038
-100º	-0.21163	-0.20338	-0.07082
-110º	-0.21657	-0.19917	-0.07158

6.4 Conclusion

To sum up, we primarily discuss the magnetic property of heteroallene and heterocumulene based *tert*-butyl nitroxide diradicals, where the latter shows *E*- and *Z*-isomers. Heteroallene based diradicals manifest ferromagnetic coupling whereas heterocumulene based diradicals show tuning of *J* values from antiferromagnetic to ferromagnetic state on going from *Z*- to *E*-isomer. The heteroatom (P/As) substitution in allene and cumulene couplers causes some geometrical changes due to the presence of lone pair of electrons on the heteroatom. Along with spin polarization, a delocalized radical unit is formed from the radical center to the coupler in all the *tert*-butyl nitroxide diradicals. The shapes of the SOMOs also assure the delocalization of unpaired electron within the coupler. Magneto-structural correlation shows that for both the *E*- and *Z*-isomers, magnetic crossover occurs at a certain range of dihedral angles depending on the spin accumulation on two nearby magnetic centers. From all these observations we conclude that the typical characteristics of *tert*-butyl nitroxide as a radical center and the presence of heteroatom within the coupler produce significant effect on our designed systems which show magnetic crossover associated with geometrical isomers in heterocumulene based systems.

6.5 References

(1) Taylor, D. R. *Chem. Rev.* **1967**, *67*, 317-359.
(2) Hendon, C.H.; Tiana, D.; Murray, A.T.; Carbery, D.R.; Walsh, A. *Chem. Sci*. **2013**, *4*, 4278–4284.
(3) Eliel, L. E.; Wilen, S. H. Stereochemistry of organic compounds; John Wiley & Sons: New York, **1994**; Chapter 9, p 539.
(4) Skibar, W.; Kopacka, H.; Wurst, K.; Salzmann, C.; Ongania, K.H.; Biani, F.F.D.; Zanello. P.; Bildstein, B. *Organometallics* **2004**, *23*, 1024-1041.
(5) Januszewski, J.A.; Tykwinski, R.R. *Chem. Soc. Rev.* **2014**, *43*, 3184-3203.
(6) Januszewski, J.A.; Wendinger, D.; Methfessel, C.D.; Hampel, F.; Tykwinski, *Angew. Chem. Int. Ed.* **2013**, *52*, 1817 –1821.
(7) Wendinger, D.; Tykwinski, R.R. *Acc. Chem. Res.* **2017**, *50*, 1468−1479.
(8) Shil, S.; Misra, A. *J. Phys. Chem. A* **2010**, *114*, 2022-2027.
(9) Bhattacharya, D.; Shil, S.; Misra, A. *J. Photochem. Photobiol., A* **2011**, *217*, 402−410.
(10) Zhang, F.; Song, X.; Bu, Y. *J. Phys. Chem. C* **2015**, *119*, 27930-27937.
(11) Saha, A.; Latif, I. A.; Datta, S.N. *J. Phys. Chem. A* **2011**, *115*, 1371-1379.
(12) Ali, Md. E.; Staemmler, V.; Illas, F.; Oppeneer, P.M. *J. Comput. Theory Chem.* **2013**, *9*, 5216-5220.
(13) Bhattacharya, D.; Misra, A. *J. Phys. Chem. A*, **2009**, *113*, 5470–5475.
(14) Shil, S.; Sarbadhikary, P.; Misra, A. *RSC Adv*. **2016**, *6*, 99467.

(15) Paul, S.; Misra, A. *J. Phys. Chem. A.* **2010**, *114*, 6641.
(16) Coey, J. M. D. Magnetism and magnetic materials, Cambridge University Press, Cambridge, U.K., **2010**, ISBN 13: 9780521816144.
(17) Latif, I. A.; Singh, V. P.; Bhattacharjee, U.; Panda, A.; Datta, S. N. *J. Phys. Chem. A* **2010**, *114*, 6648–6656.
(18) Ali, Md. E.; Datta, S.N. *J. Phys. Chem. A* **2006**, *110*, 2776-2784.
(19) Cho, D.; Ko, K. C.; Ikabata, Y.; Wakayama, K.; Yoshikawa, T.; Nakai, H.; Lee, J.Y. *J. Chem. Phys.* **2015**, *142*, 024318.
(20) Kolanji, K.; Postulka, L.; Wolf, B.; Lang, M.; Schollmeyer, D.; Baumgarten. M. *J. Org. Chem.* **2019**, *84*, 140−149.
(21) Song, M.; Song, X.; Bu, Y. *Chem. Phys. Chem.* **2017**, *18*, 2487-2498.
(22) Chen, D.; Deng, T.; Yang, L.; Bu, Y. *J. Phys. Chem. C* **2019**, *123*, 14152−14163.
(23) Sarbadhikary, P.; Shil, S.; Panda, A.; Misra, A. *J. Org. Chem*, **2016**, *81*, 5623.
(24) Sarbadhikary, P.; Shil, S.; Misra, A. *Phys. Chem. Chem. Phys.* **2018**, *20*, 9364-9375.
(25) Garner, M. H.; Hoffmann, R.; Rettrup, S.; Solomon, G.C. *ACS Cent. Sci.***2018**, *4*, 688-700.
(26) Garner, M. H.; Jensen, A.; Hyllested, L.; Solomon, G. C. *Chem. Sci.* **2019**, ***10***, 4598-4608.
(27) Aoki, Y.; Orimoto, Y.; Imamura, A. *ACS Cent. Sci.* **2018**, 4, 664-665.
(28) Appel, R. Multiple Bonds and Low Coordination in Phosphorus Chemistry, Georg Thieme Verlag: Stuttgart, Germany, **1990**; p 157.
(29) Escudié, J.; Ranaivonjatovo, H.; Rigon, L. *Chem. Rev.* **2000**, *100*, 3639-3696.
(30) Eichler, B.; West, R. *Adv. Organomet. Chem.* **2000**, *46*, 1-46.
(31) Escudié, J.; Ranaivonjatovo, H.; Bouslikhane, M.; Harouch, Y. E; Baiget, L.; Nemes, G.C. *Russ. Chem. Bull., Int. Ed.* **2004**, *53*, 1020-1033.
(32) Escudié, J.; Ranaivonjatovo, H. *Organometallics* **2007,** *26*, 1542-1559.
(33) Märkl, G.; Sejpka, H.; Dietl, S.; Nuber, B.; Ziegler, M. L. *Angew. Chem., Int. Ed. Engl*. **1986**, *25*, 1003-1004.
(34) Bouslikhane, M.; Gornitzka, H.; Ranaivonjatovo, H.; Escudié, J. *Organometallics* **2002**, *21*, 1531-1533.
(35) Rancurel, C.; Heise, H.; Köhler, F. H.; Schatzschneider, U.; Rentschler, E.; Vidal-Gancedo, J.; Veciana, J.; Sutter, J. –P. *J. Phys. Chem. A* **2004**, *108*, 5903-5914.
(36) Polo, V.; Alberola, A.; Andres, J.; Anthony, J.; Pilkington, M. *Phys. Chem. Chem. Phys.* **2008**, *10*, 857–864.
(37) Bhattacharya, D.; Shil, S.; Panda, A.; Misra, A. *J. Phys. Chem. A* **2010**, *114*, 11833–11841.

(38) Tamura, M.; Nakazawa, Y.; Shiomi, D.; Nozawa, K.; Hosokoshi, Y.; Ishikawa, M.; Takahashi, M.; Kinoshita, M. *Chem. Phys. Lett.* **1991**, *186*, 401-404.
(39) Ziessel, R.; Stroh, C.; Heise, H.; Köhler, F. H.; Turek, P.; Claiser, N.; Souhassou, M.; Lecomte, C. *J. Am. Chem. Soc.* **2004**, *126*, 12604-12613.
(40) Hicks, R. G.; Lemaire, M. T.; Öhrström, L.; Richardson, J. F.; Thompson, L. K.; Xu, Z. *J. Am. Chem. Soc*. **2001**, *123*, 7154-7159.
(41) Wautelet, P.; Catala, L.; Bieber, A.; Turek, P.; André, J.-J. *Polyhedron* **2001**, *20*, 1571-1576.
(42) Gomberg, M. *J. Am. Chem. Soc*. **1900**, *22*, 757-771.
(43) Gomberg, M. *Chem. Rev*. **1924**, *1*, 91-141.
(44) Kanno, F.; Inoue, K.; Koga, N.; Iwamura, H. *J. Am. Chem. Soc.***1993**, *115,* 847-850.
(45) Calder, A,; Forester, A. R.; James, P. *G.;* Luckhurst, G. R. *J. Am. Chem. Soc.* **1969**, *91,* 3724-3727.
(46) Fang, S.; Lee, M. –S.; Hrovat, D.A.; Borden, W.T. *J. Am. Chem. Soc.* **1995,** *117***,** 6727-6731.
(47) Jung, M.; Sharma, A.; Hinderberger, D.; Braun, S.; Schatzschneider, U.; Rentschler, E. *Inorg. Chem.* **2009**, *48*, 7244–7250.
(48) Oniciu, D. C.; Matsuda, K.; Iwamura, H. *J. Chem. Soc., Perkin Trans.* **1996**, *2*, 907-913.
(49) Inoue, K.; Iwamura, H. *J. Am. Chem. Soc.***1994,** *116***,** 3173-3174.
(50) Noodleman, L. *J. Chem. Phys.***1981**, *74*, 5737−5743.
(51) Noodleman, L.; Baerends, E. J. *J. Am. Chem. Soc.* **1984**, *106*, 2316−2327.
(52) Noodleman, L.; Davidson, E. R. *Chem. Phys.***1986**, *109*, 131−143.
(53) Noodleman, L.; Peng, C. Y.; Case, D. A.; Mouesca, J. -M. *Coord. Chem. Rev.***1995**, *144*, 199−244.
(54) Martin, R. L.; Illas, F. *Phys. Rev. Lett.* **1997**, *79*, 1539-1542.
(55) Caballol, R.; O. Castell, O.; Illas, F.; Moreira, I. de P. R.; Malrieu, J. P. *J. Phys. Chem. A* **1997**, *101*, 7860-7866.
(56) Paul, S.; Misra, A. *J. Chem. Theory Comput.* **2012**, *8*, 843−853.
(57)Yamaguchi, K.; Fukui, H.; Fueno, T. *Chem. Lett.* **1986**, *15*, 625−628.
(58) Yamaguchi, K.; Takahara, Y.; Fueno, T.; Nasu, K. *Jpn. J. Appl. Phys.***1987**, *26*, L1362−L1364.
(59) Yamaguchi, K.; Jensen, F.;Dorigo, A.; Houk, K. N. *Chem. Phys. Lett.* **1988**, *149*, 537−542.
(60) Yamaguchi, K.; Takahara, Y.; Fueno, T.; Houk, K. N. *Theor. Chim. Acta.* **1988**, *73*, 337−364.
(61) Frisch, M. J.; Trucks, G. W.; Schlegel, H. B.; Scuseria, G. E.; Robb, M. A.; Cheeseman, J. R.; Scalmani, G.; Barone, V.; Mennucci, B.; Petersson, G. A.; Nakatsuji, H.; Caricato, M.; Li, X.; Hratchian, H. P.; Izmaylov, A. F.; Bloino, J.; Zheng, G.; Sonnenberg, J. L.; Hada, M.; Ehara, M.; Toyota, K.; Fukuda, R.; Hasegawa, J.; Ishida, M.; Nakajima, T.; Honda, Y.; Kitao, O.; Nakai, H.; Vreven, T.; Montgomery, J. A., Jr.; Peralta, J. E.; Ogliaro, F.; Bearpark, M.; Heyd, J. J.; Brothers, E.; Kudin, K. N.; Staroverov, V. N.; Kobayashi, R.; Normand, J.; Raghavachari, K.;

Rendell, A.; Burant, J. C.; Iyengar, S. S.; Tomasi, J.; Cossi, M.; Rega, N.; Millam, M. J.; Klene, M.; Knox, J. E.; Cross, J. B.; Bakken, V.; Adamo, C.; Jaramillo, J.; Gomperts, R.; Stratmann, R. E.; Yazyev, O.; Austin, A. J.; Cammi, R.; Pomelli, C.; Ochterski, J. W.; Martin, R. L.; Morokuma, K.; Zakrzewski, V. G.; Voth, G. A.; Salvador, P.; Dannenberg, J. J.; Dapprich, S.; Daniels, A. D.; Farkas, Ö.; Foresman, J. B.; Ortiz, J. V.; Cioslowski, J.; Fox, D. J. Gaussian, Inc., Wallingford CT, **2009**.

(62) Shil, S.; Herrmann, C. *Inorg. Chem.* **2015**, *54*, 11733–11740.

(63) Ali, M. E.; Roy, A. S.; Datta, S. N. *J. Phys. Chem. A* **2007**, *111*, 5523–5527.

(64) Polo, V.; Alberola, A.; Andres, J.; Anthony, J.; Pilkington, M. *Phys. Chem. Chem. Phys*. **2008**, *10*, 857-864.

(65) Shil, S.; Roy, M.; Misra, A. *RSC Adv*. **2015**, *5*, 105574-105582.

(66) Herring, C. in Magnetism IIB, Direct exchange between well-separated atoms, ed. G.T. Rado and H. Suhl, Academic Press, New York, **1966**, vol. 5.

(67) Trindle, C.; Datta, S. N. *Int. J. Quantum Chem.***1996**, *57*, 781-799.

(68) Schatzschneider, U.; Rentschler, E. *J. Mol. Struct. (Theochem)* **2003**, 638, 163–168.

(69) Hoffmann, R.; Zeiss, G. D.; Dine, G. W. V. *J. Am. Chem. Soc*. **1968**, *90*, 1485.

(70) Zhang, G.; Li, S.; Jiang, Y. *J. Phys. Chem. A* **2003**, *107*, 5573-5582.